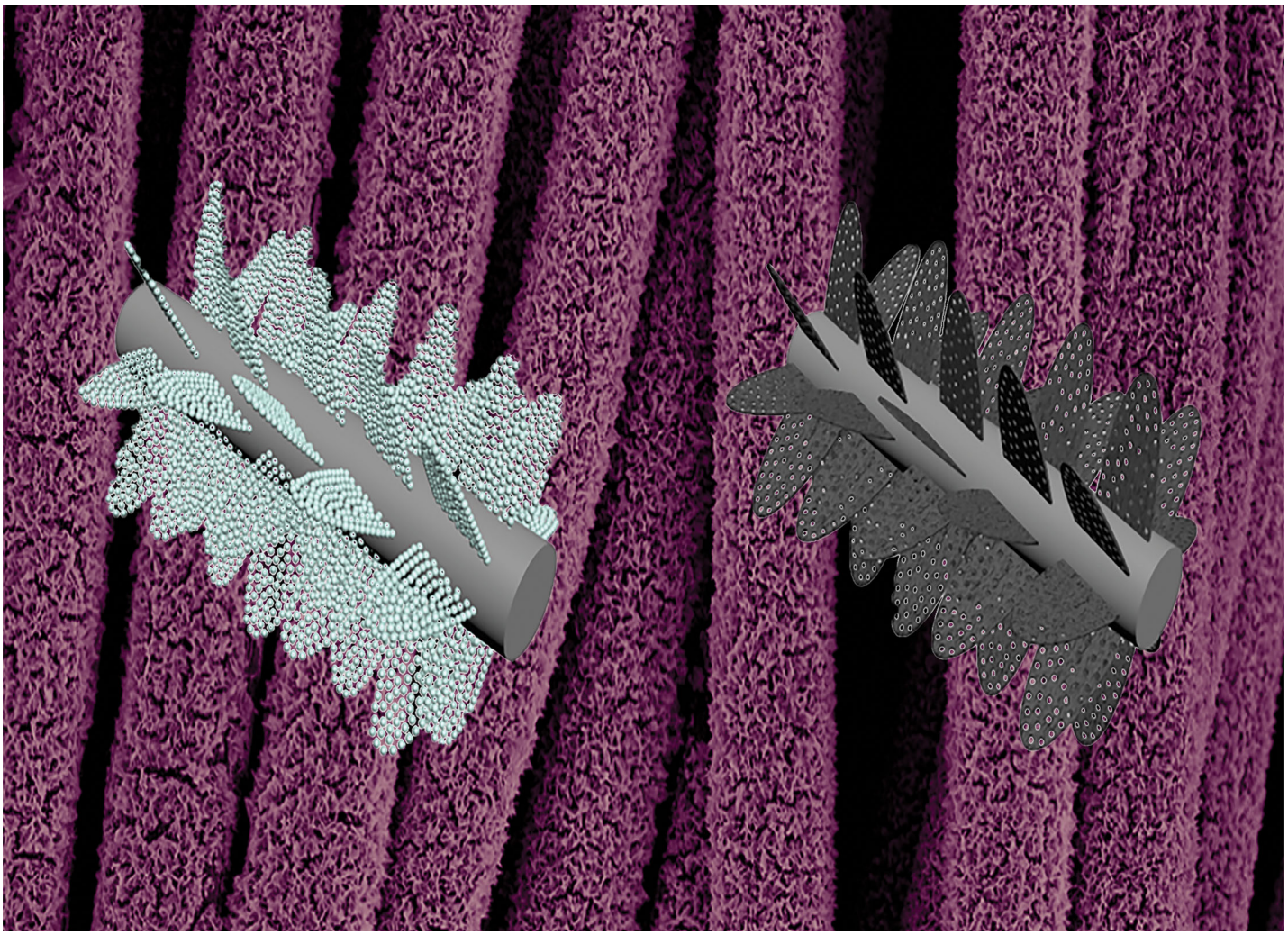

Showcasing research from Professor John Wang's group, Department of Materials Science and Engineering, National University of Singapore, Singapore

Cobalt oxide and N-doped carbon nanosheets derived from a single two-dimensional metal–organic framework precursor and their application in flexible asymmetric supercapacitors

A single two-dimensional metal–organic framework (MOF) precursor can be steadily transformed into both electrodes (Co_3O_4 cathode and N-doped carbon anode) for a flexible asymmetric supercapacitor, based on a new "one for two" strategy, which can greatly ease the fabrication process of a full device and can be extended to prepare various functional materials for advanced integrated devices.

As featured in:

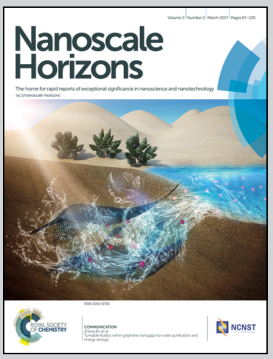

See Cao Guan, Anthony K. Cheetham, John Wang *et al.*, *Nanoscale Horiz.*, 2017, **2**, 99.

ROYAL SOCIETY OF CHEMISTRY

rsc.li/nanoscale-horizons

Registered charity number: 207890

Nanoscale Horizons

COMMUNICATION

View Article Online
View Journal | View Issue

Cite this: *Nanoscale Horiz.*, 2017, 2, 99

Received 14th December 2016,
Accepted 17th January 2017

DOI: 10.1039/c6nh00224b

rsc.li/nanoscale-horizons

Cobalt oxide and N-doped carbon nanosheets derived from a single two-dimensional metal–organic framework precursor and their application in flexible asymmetric supercapacitors†

Cao Guan,*[a] Wei Zhao,[b] Yating Hu,[a] Zhuangchai Lai,[b] Xin Li,[a] Shijing Sun,[c] Hua Zhang,[b] Anthony K. Cheetham*[ac] and John Wang*[a]

Based on a new "one for two" strategy, a single two-dimensional (2D) metal–organic framework (MOF) precursor has been transformed into both electrodes (*i.e.*, a Co_3O_4 cathode and a N-doped carbon anode) for a flexible asymmetric supercapacitor. The device demonstrated not only highly robust mechanical flexibility but also outstanding electrochemical performance. The "one for two" concept can significantly ease the fabrication process and has great potential to be extended to other functional materials for different applications.

Conceptual insights

Supercapacitors with high energy density and flexibility are highly desired for the development of advanced flexible electronics. Most of the previous reports on asymmetric supercapacitors need two different precursors for the respective anode and cathode, thus the fabrication process is rather complicated. Herein, an effective "one for two" strategy is used to construct the "two" nanoporous electrodes of a flexible asymmetric supercapacitor from just "one" precursor. To specify, both electrode materials, *i.e.* a porous cobalt oxide nanosheets cathode (CC@Co_3O_4) and a porous nitrogen-doped carbon nanosheets anode (CC@NC) can be transformed from a single 2D cobalt MOF. Due to the advantages of the MOF-derived nanoporous electrode materials, and their direct contact with the flexible substrates, the asymmetric supercapacitor expressed high specific energy densities with excellent mechanical stability. The "one for two" strategy can greatly ease the fabrication process of a full device and can be extended to design other advanced integrated devices.

MOFs represent a new class of hybrid nanoporous materials with crystalline architectures, highly tunable porosities and different functionalities for a wide variety of applications.[1–7] Recently, MOFs have been utilized for electrical energy storage (EES) devices, taking the advantage of their intrinsically large surface areas with sufficient reaction sites for redox reactions.[8–10] They can be directly used as electrode materials for lithium-ion batteries and supercapacitors,[11] and through proper post-synthesis treatment, MOFs can also be readily transformed to porous carbons, metal oxides, and metal sulfides as active materials for energy storage.[12–20] In particular, two-dimensional nanostructured MOFs have attracted considerable scientific and technological interest, because of their low dimensionality with unique physical and chemical properties.[21–26] However, most of the previous research work on MOF-based materials has focused only on one of the electrodes (*e.g.* anode for lithium ion batteries or cathode for supercapacitors), thus to assemble a full cell additional efforts are needed on a second material for the other electrode. Furthermore, most of the MOF or MOF-derived active materials are in powdered form, where the usage of polymer binders will increase the "dead mass" for the electrodes and limit the gravimetric/volumetric capacity of the full device.[27–31] Last but not least, with the rapid development of portable and flexible electronics, such as roll-up displays and curved smartphones, it is of considerable value to explore flexible and environmental friendly EES devices.[32–35]

For EES devices, batteries and electrochemical capacitors are playing dominant roles.[36] Compared with lithium-ion batteries, supercapacitors can offer much higher power densities ($\sim$10 kW kg^{-1}) with shorter charging times (within 1 min), and the cycle life ($>$100 000 cycles) is also much longer.[37] However, the energy densities of supercapacitors are normally low ($\sim$15 W h kg^{-1} to 35 W h kg^{-1}), which limits their potentially wide applications in areas such as hybrid electric vehicles and portable electronics.[38] To address this issue, one direction for high-energy-density supercapacitors is to develop flexible binder-free electrodes, which can avoid the "dead" mass of binders and provide direct mechanical and electrical contacts between the active materials and substrates.[39–44] In addition, constructing hybrid supercapacitors is also a promising way to

[a] *Department of Materials Science and Engineering, National University of Singapore, 117574 Singapore. E-mail: msegc@nus.edu.sg, msewangj@nus.edu.sg*
[b] *School of Materials Science and Engineering, Nanyang Technological University, 639798 Singapore*
[c] *Department of Materials Science and Metallurgy, University of Cambridge, Cambridge, CB2 3QZ, UK. E-mail: akc30@cam.ac.uk*

† Electronic supplementary information (ESI) available: Detailed experimental procedures, additional XRD pattern, SEM images, TEM images, digital photos, XPS results of MOF precursor and the derived products, and additional electrochemical characterization. See DOI: 10.1039/c6nh00224b

achieve high energy densities, as the voltage window can be significantly expanded.[45,46] Generally, in an asymmetric supercapacitor, the two electrodes are quite different, thus it would be intriguing and also promising if the two electrodes could be derived from a single-source precursor. In this way, the two electrodes will not only share similar properties (*e.g.* porosity and flexibility), but also offer possible synergetic effects with different physiochemical properties. The "one for two" and "one for all" strategy can also simplify the fabrication process to reduce the cost, and thus has great potential for the development of various functional materials for different integrated devices. Based on the above discussion, it would be of considerable interest to develop different functional materials from a single MOF precursor and assemble them into a well-integrated device.

In this work, we develop a facile approach to directly grow 2D MOFs on flexible substrates; through different thermal treatments they can then be transformed to metal oxides and carbon, suitable for the cathode and anode of an asymmetric supercapacitor, respectively. As a proof-of-concept demonstration of the "one for two" strategy, a solid-state flexible supercapacitor is assembled based on the single MOF precursor-derived cathode and anode, and excellent electrochemical performance, such as high energy density and high power density, is achieved. The solid-state supercapacitor also demonstrates good mechanical stability with long-time cycling stability. The proposed "one for two" strategy for the development of porous 2D metal oxides and carbon can be extended to other MOF-based functional materials for different integrated devices.

The fabrication process of the electrode materials and the architecture of the flexible asymmetric supercapacitor are schematically illustrated in Fig. 1. Firstly, though a facile reaction between Co^{2+} and 2-methylimidazole (MIM, $C_4H_6N_2$) in aqueous solution, a 2D sheet-like Co-MOF was directly grown on the surface of carbon macro-fiber of the carbon cloth (noted as CC@Co-MOF). X-ray powder diffraction data, analyzed using Pawley refinement with the Topas program (Fig. S1, ESI†), showed that the Co-MOF has the same 2D layered crystal structure as its known zinc analogue.[16,47] (Pawley refinement details are in the ESI.†) Then, through different thermal treatment processes, the Co-MOF precursor can be either oxidized to Co_3O_4 nanosheets (CC@Co_3O_4) or transformed to N-doped porous carbon nanosheets (CC@NC) (see Experimental in ESI† for details). In a final step, a flexible asymmetric supercapacitor is assembled using the CC@Co_3O_4 cathode and the CC@NC anode with a poly(vinyl alcohol) (PVA)–KOH gel-electrolyte. Note that the MOF coating is very uniform and that the facile fabrication process can thus be easily scaled up on different substrates such as FTO, graphite foam, Ti foil, and nickel foam (refer to Fig. S2 and S3, ESI†), here we just focus on the carbon cloth substrate as a demonstration of principle.

The scanning electron microscopy (SEM) image in Fig. S4 (ESI†) shows that Co-MOFs with a typical 2D morphology (length ~1.5 μm and thickness of ~100–150 nm) have been uniformly grown on the carbon cloth. To transform the Co-MOF into Co_3O_4, the CC@Co-MOF was stabilized in N_2 and then oxidized in air. Digital images and large-scale SEM

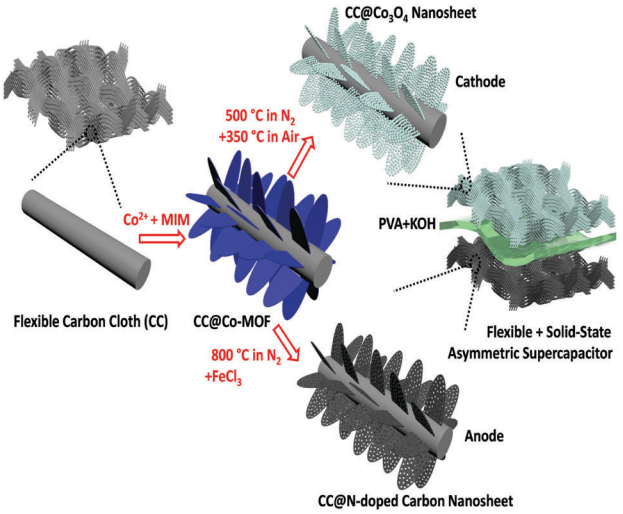

Fig. 1 Schematic illustration of the "one for two" fabrication process: 2D Co_3O_4 nanosheets cathode and N-doped carbon nanosheets anode are obtained from the same Co-MOF precursor and assembled into a flexible asymmetric supercapacitor.

images of CC@Co_3O_4 in Fig. S5 (ESI†) shows the uniform coverage of Co_3O_4 after thermal treatment. The MOF precursor will decompose and react with O_2 releasing gas molecules such as NH_3, H_2O and CO_2 during the annealing process, thus the resultant Co_3O_4 nanosheets become much thinner compared with the precursor (Fig. 2a), yet the 2D vertical aligned structure can be largely kept with no apparent collapse. Although the Co_3O_4 nanosheets are slightly tilted, the vertical alignment with cross-linked features was well retained, which could facilitate the electrolyte penetration. The enlarged SEM image in Fig. 2b and the transmission electron microscopy (TEM) image in Fig. 2c clearly show that the 2D Co_3O_4 nanosheets are highly porous and consist of many tightly interconnected nanoparticles (less than 10 nm). A top view of 2D Co_3O_4 indicates a typical thickness of the nanoflakes of ~50 nm (Fig. S5f, ESI†). The porous structure of the Co_3O_4 nanosheets is believed to provide high electrode–electrolyte contact, reduced ion diffusion length, and effectively buffer the volume change during electrochemical reactions.[48] The selected area electron diffraction (SAED) pattern (Fig. 2d) reveals the cubic crystalline structure of the Co_3O_4 nanosheets (JCPDS # 42-1467), and the HRTEM image in Fig. 2e shows that the spacings of the lattice fringes (0.244 nm and 0.286 nm) match well with the *d*-spacings of the (311) and (220) planes of Co_3O_4.[49] The chemical composition of the Co_3O_4 nanosheets is further illustrated by the high-angle annular dark-field (HAADF)-scanning transmission electron microscopy (STEM) image (Fig. 2f) with the corresponding elemental mapping images (Fig. 2g and h). From the mapping result, the elements of Co and O are uniformly distributed, further confirming the successful formation of porous Co_3O_4 nanosheets.

The Co-MOFs can be also easily transformed to N-doped carbon nanosheets through N_2 thermal treatment with the following $FeCl_3$ etching process. As shown in Fig. 2a′ and b′, after the transformation, the N-doped carbon nanosheets maintained

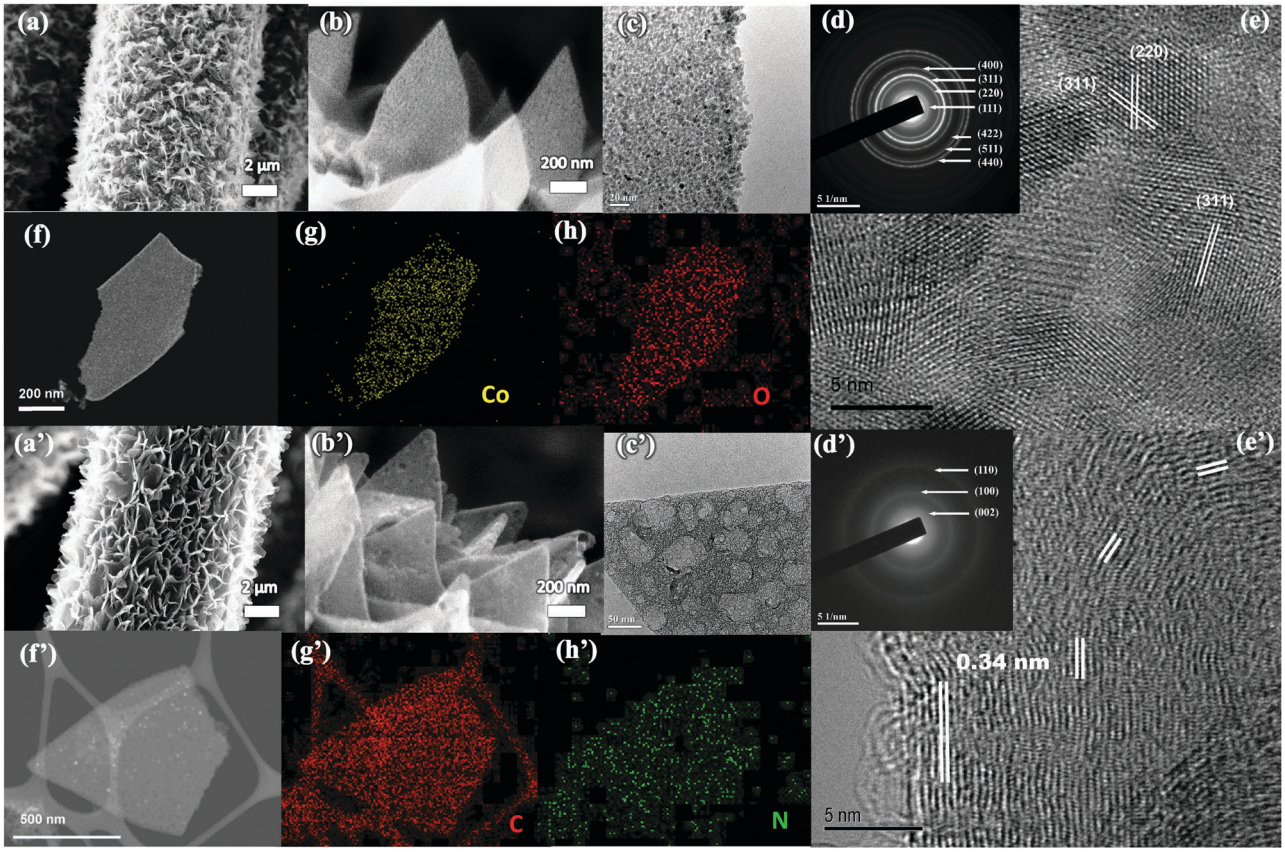

Fig. 2 (a and b) SEM images, (c) TEM image, (d) SAED pattern, (e) HRTEM image, (f) HAADF-STEM image, (g and h) EDX mapping result of Co_3O_4 nanosheets deposited on CC. (a′ and b′) SEM images, (c′) TEM image, (d′) SAED pattern, (e) HRTEM image, (f′) HAADF-STEM image, (g′ and h′) EDX mapping result of porous N-doped carbon nanosheets deposited on CC.

uniform coverage on the carbon cloth, and the thickness (~70 nm) of the carbon nanosheets is a little larger than that of the Co_3O_4 (Fig. S5g, ESI†). Fig. 2c′ shows a representative TEM image of a porous carbon nanosheet, in which both meso- and macro-pores can be observed. The porous feather is believed to facilitate the electrode–electrolyte contact.[50] The SAED pattern in Fig. 2d′ reveals the graphitic feature of the carbon nanosheets, and the lattice spacing in Fig. 2e′ can be assigned to the (200) plane of graphitic carbon.[51–53] The HAADF-STEM image (Fig. 2f′) with the corresponding elements (N and C) mapping results in Fig. 2g′ and h′ also confirm the uniform distribution of N and C, and proves the formation of N-doped carbon nanosheets. Note that the N_2 thermal treatment of the Co-MOF results in a Co/carbon composite (refer to TEM images in Fig. S6, ESI†), and in the current work we use $FeCl_3$ aqueous solution (instead of hazardous HF) to successfully etch away most of the Co.

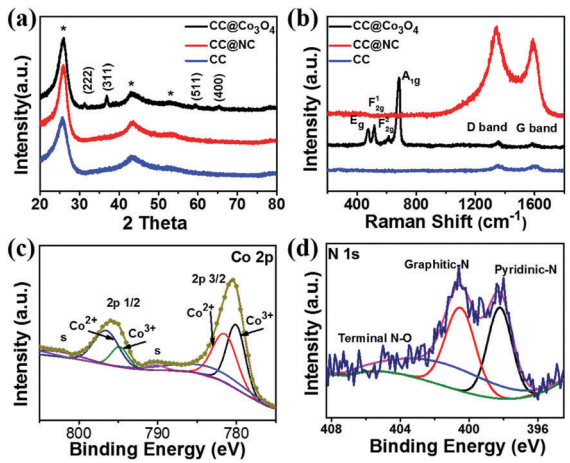

Fig. 3 (a) XRD and (b) Raman results of CC, CC@Co_3O_4 and CC@NC. XPS spectra of (c) Co 2p in CC@Co_3O_4 and (d) N 1s in CC@NC.

XRD, Raman, and X-ray photoelectron spectroscopy (XPS) have been carried out to investigate the compositions of CC@Co_3O_4 and CC@NC. As shown in Fig. 3a, excluding the peaks from the carbon cloth substrate (CC), all the other diffraction peaks obtained from CC@Co_3O_4 can be well indexed as Co_3O_4 (JCPDS # 42-1467).[49,54] From the Raman spectrum in Fig. 3b, in addition to the D band and G band signals from the carbon support, the Raman bands located at 478, 519, 616 and 685 cm^{-1} can be assigned to the E_g, F^1_{2g}, F^2_{2g}, and A_{1g} modes of Co_3O_4, respectively. Fig. 3c shows the Co 2p XPS spectrum collected from CC@Co_3O_4, in which the two main peaks located at ~780.5 and 795.9 eV, each accompanied by a shake-up satellite peak with low intensity, can be attributed to Co $2p_{3/2}$ and Co $2p_{1/2}$ of pure Co_3O_4, respectively.[55–58] From the XPS result in Fig. 3d, the signals of pyridinic-N, graphitic-N, and terminal N–O bonding further

confirms the nitrogen doping of the carbon nanosheets, which is in accordance with previous reports on ZIF derived N-doped carbon.[59,60] The wide survey XPS spectra of CC@Co_3O_4 and CC@NC can be found in Fig. S7 (ESI†).

Based on the above discussion, a single 2D MOF precursor can be successfully transformed to both porous Co_3O_4 nanosheets and nitrogen-doped porous carbon nanosheets, which are promising electrode materials for supercapacitors. To evaluate the electrochemical performance of the CC@Co_3O_4 cathode and CC@NC anode as an asymmetric supercapacitor, electrochemical tests were first conducted using a three-electrode system in KOH aqueous electrolyte, with Pt as the counter electrode and Hg/HgO as the reference electrode. Fig. 4a compares the cyclic voltammetry (CV) curves of the CC@Co_3O_4 at different scan rates from 10 to 100 mV s^{-1}. One pair of apparent oxidation (at ~0.55 V) and reduction (at ~0.45 V) peaks can be observed, suggesting reversible Faradaic reaction between Co^{2+} and Co^{3+} associated with OH^-.[61–63] Note that the symmetric redox peaks do not shift much when the scan rate increases from 10 to 100 mV S^{-1}, showing that the electrode has good reaction kinetics. Noting the voltage window at 100 mV s^{-1} is enlarged a little to fully express the oxidation peak. The reversible reaction of CC@Co_3O_4 is further confirmed by the galvanostatic charge–discharge (GCD) curves in Fig. S8a (ESI†), in which a charge plateau at ~0.51 V and a discharge plateau at ~0.47 V can be observed, reflecting a small voltage hysteresis of only ~0.04 V. Based on the GCD curves, the capacitances at different current densities are readily determined. It is found that the CC@Co_3O_4 shows the highest specific capacity of ~900 F g^{-1} (corresponding to ~0.225 mF cm^{-2}) at 10 A g^{-1}, and 58.7% of this value can be maintained when the current density is increased 16 times (Fig. S8b, ESI†), demonstrating the excellent rate performance. Electrochemical impedance spectroscopy (EIS) in Fig. S8c (ESI†) further demonstrates a small charge transfer resistance (~0.3 Ω) of the electrode. The high capacity and excellent rate performance of the CC@Co_3O_4 electrode are due to the highly porous Co_3O_4 nanosheets with ultrathin thickness and their direct electrical contact with the conductive carbon cloth support.

Similarly, the electrochemical performance of the CC@NC anode was studied in the same three-electrode system. From the near-rectangular CV curves in Fig. 4b (results at higher scan rates are shown in Fig. S9a, ESI†) and triangular GCD curves in Fig. S9b (ESI†), the CC@NC electrode shows a typical non-Faradaic double-layer behavior with good charge transfer.[64] At a current density of 6.25 A g^{-1}, the CC@NC shows a specific capacitance of 321.9 F g^{-1}, which is evidently higher than those of powdered porous carbon materials.[65–67] Note that 80.8% of the capacitance can be maintained when the current is increased 16 times (Fig. S9c, ESI†), and that the EIS curve in Fig. S9d (ESI†) demonstrates the excellent conductivity of the CC@NC electrode. The good electrochemical performance of the NC probably arises from the N-doping and porous features, together with its vertical aligned 3D structure which has direct contact with the carbon support.[68]

A flexible asymmetric supercapacitor using the CC@Co_3O_4 cathode, CC@NC anode and a PVA–KOH electrolyte was assembled and typical CV curves are shown in Fig. 4c. The CV curves are quasi-rectangular and symmetrical in shape without sharp redox peaks, even at the high scan rate of 100 mV, indicating that CC@Co_3O_4//CC@NC has ideal capacitive properties with good reversibility. Fig. 4d shows typical charge and discharge curves of the asymmetric supercapacitor at different current densities from 7.7 to 61.5 A g^{-1}; all the curves demonstrate almost linear charge–discharge characteristics, confirming the ideal capacitive properties of the full-cell. At a current density of 7.7 A g^{-1}, the

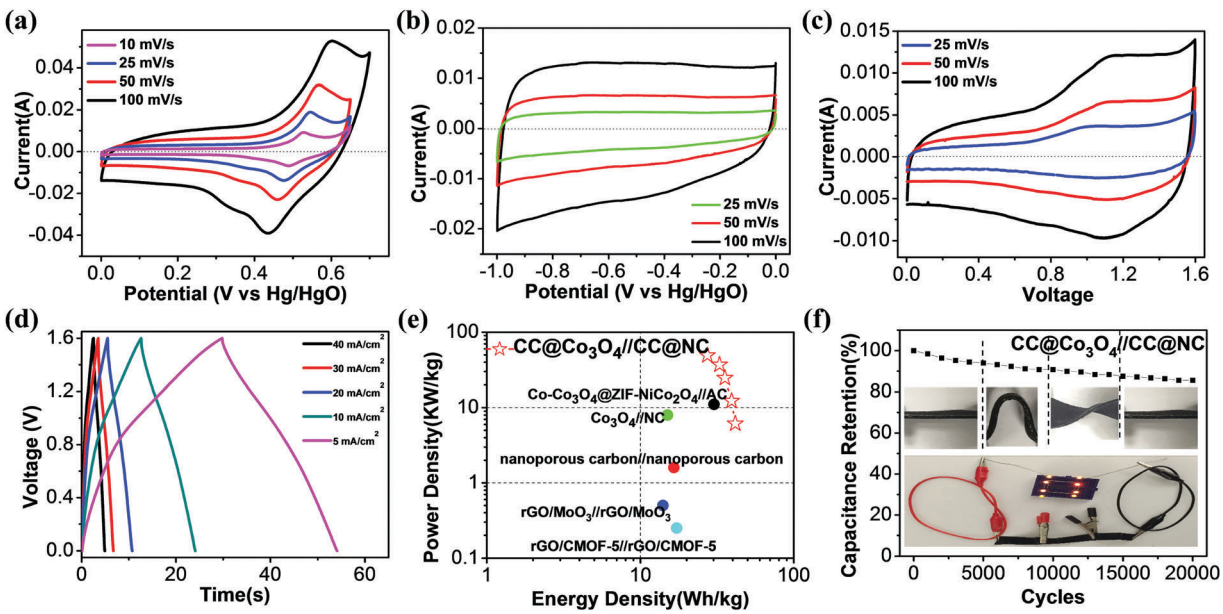

Fig. 4 CV curves of (a) CC@Co_3O_4, (b) CC@NC, (c) CC@Co_3O_4//CC@NC; (d) charge–discharge curves, (e) Ragone plots, and (f) cycling test result of the asymmetric supercapacitor with PVA–KOH gel electrolyte. Insert in (f) shows digital images of the flat, bending, and twisting states of the cell during cycling test (upper) and a demo that three full cells (each size of 1 × 2.5 × 0.08 cm^3) can light up 8 orange LEDs.

asymmetric supercapacitor delivers a capacity of $\sim$116.8 F g^{-1}, and it only decreases to $\sim$76.9 F g^{-1} when the current density is increased 8 times, showing fast kinetic behavior. The high rate properties of the asymmetric supercapacitor could arise from: (i) the nanoporous structure of the electrodes which provide high surface areas and short ion diffusion lengths, and (ii) the direct contact between the active materials and the carbon support, which provides a good electron transport highway. A Ragone plot (power (*P*) *vs.* energy (*E*) density) of the CC@Co_3O_4//CC@NC is given in Fig. 4e, with data obtained from other MOF-based solid-state supercapacitors inserted for comparison. The CC@Co_3O_4//CC@NC device demonstrated performance comparable to the previously reported MOF-based supercapacitors;[13,27,69–71] it delivers a maximum energy density of 41.5 W h kg^{-1} at a power density of 6.2 kW kg^{-1}, and it maintains 27.4 W h kg^{-1} at a peak power density of 49.2 kW kg^{-1}. When the mass of the whole system (including the carbon cloth substrate) is calculated, the maximum energy and power density decrease to 1.3 W h kg^{-1} and 1.55 kW kg^{-1}, respectively, due to the heavy carbon cloth substrate. Here we just use carbon cloth as a typical prototype demonstration, and the energy and power density of the full cell can be further improved with an optimized flexible and light-weight support. The long-term cycling stability and stable mechanical flexibility of the asymmetric supercapacitor were also tested. As shown in Fig. 3f, even when the CC@Co_3O_4//CC@NC full-cell was under different bending/twisting conditions (insert in Fig. 4f) during the cycling test, it still retains 90.8% and 85.5% of the initial capacity after 10 000 and 20 000 cycles, respectively, showing structural stability with excellent cycling durability. The capacity fading can be from the structure change, volume expansion during the cycling, however, this retention of performance compares favorably with results that have been reported for other CoO_x based supercapacitors.[57,62,72–74] The potential usage of the solid-state full-cell for flexible/bendable electronics is further demonstrated, as shown in the insert of Fig. 3f, whereby eight orange LEDs can be lit by three connected asymmetric supercapacitors ($3 \times 2.5 \times 0.08$ cm^3) under bending states.

Conclusions

To conclude, based on a new "one for two" strategy, a 2D MOF has been directly grown on conductive substrates, and through different thermal treatment it can be steadily transformed to porous metal oxide and carbon, suitable for both electrodes in an asymmetric supercapacitor configuration. Due to the highly porous electrodes and their direct contact with the flexible substrates, the flexible solid-state supercapacitor demonstrated both high electrochemical performance and high mechanical stability. The "one for two" strategy can be extended to other functional materials for different integrated devices, *e.g.*, MOFs for different porous metal oxides/sulfides and carbon materials for energy and environment applications.

Acknowledgements

This work is supported by the Ministry of Education, Grant number: MOE2015-T2-2-094, conducted at the National University of Singapore. This work was supported by MOE under AcRF Tier 2 (ARC 26/13, No. MOE2013-T2-1-034; ARC 19/15, No. MOE2014-T2-2-093; MOE2015-T2-2-057) and AcRF Tier 1 (RG5/13), and NTU under Start-Up Grant (M4081296.070.500000) in Singapore. This research is supported by the National Research Foundation, Prime Minister's Office, Singapore under its Campus for Research Excellence and Technological Enterprise (CREATE) programme. The authors also thank Dr Yue Wu from University of Cambridge for fruitful discussions and help on XRD analysis.

References

1 P. Pachfule, D. Shinde, M. Majumder and Q. Xu, *Nat. Chem.*, 2016, **8**, 718–724.
2 I. Stassen, M. Styles, G. Grenci, H. V. Gorp, W. Vanderlinden, S. D. Feyter, P. Falcaro, D. D. Vos, P. Vereecken and R. Ameloot, *Nat. Mater.*, 2015, **15**, 304–310.
3 S. Bai, X. Liu, K. Zhu, S. Wu and H. Zhou, *Nat. Energy*, 2016, **1**, 16094.
4 H. Furukawa, K. E. Cordova, M. O'Keeffe and O. M. Yaghi, *Science*, 2013, **341**, 1230444.
5 A. A. Talin, A. Centrone, A. C. Ford, M. E. Foster, V. Stavila, P. Haney, R. A. Kinney, V. Szalai, F. El Gabaly, H. P. Yoon, F. Léonard and M. D. Allendorf, *Science*, 2014, **343**, 66–69.
6 J. Long, K. Shen, L. Chen and Y. Li, *J. Mater. Chem. A*, 2016, **4**, 10254–10262.
7 W.-J. Li, M. Tu, R. Cao and R. A. Fischer, *J. Mater. Chem. A*, 2016, **4**, 12356–12369.
8 L. Wang, Y. Han, X. Feng, J. Zhou, P. Qi and B. Wang, *Coord. Chem. Rev.*, 2016, **307**(Part 2), 361–381.
9 A. Morozan and F. Jaouen, *Energy Environ. Sci.*, 2012, **5**, 9269–9290.
10 Y. Zhao, Z. Song, X. Li, Q. Sun, N. Cheng, S. Lawes and X. Sun, *Energy Storage Mater.*, 2016, **2**, 35–62.
11 X.-W. Liu, T.-J. Sun, J.-L. Hu and S.-D. Wang, *J. Mater. Chem. A*, 2016, **4**, 3584–3616.
12 F.-S. Ke, Y.-S. Wu and H. Deng, *J. Solid State Chem.*, 2015, **223**, 109–121.
13 D. Yu, B. Wu, L. Ge, L. Wu, H. Wang and T. Xu, *J. Mater. Chem. A*, 2016, **4**, 10878–10884.
14 H. Hu, J. Zhang, B. Guan and X. W. Lou, *Angew. Chem.*, 2016, **128**, 9666–9670.
15 G. Zhang, S. Hou, H. Zhang, W. Zeng, F. Yan, C. C. Li and H. Duan, *Adv. Mater.*, 2015, **27**, 2400–2405.
16 G. Fang, J. Zhou, C. Liang, A. Pan, C. Zhang, Y. Tang, X. Tan, J. Liu and S. Liang, *Nano Energy*, 2016, **26**, 57–65.
17 X. Cao, B. Zheng, X. Rui, W. Shi, Q. Yan and H. Zhang, *Angew. Chem., Int. Ed.*, 2014, **53**, 1404–1409.
18 K. Xi, S. Cao, X. Peng, C. Ducati, R. Vasant Kumar and A. K. Cheetham, *Chem. Commun.*, 2013, **49**, 2192–2194.
19 A. Aijaz, J. Masa, C. Rösler, W. Xia, P. Weide, A. J. R. Botz, R. A. Fischer, W. Schuhmann and M. Muhler, *Angew. Chem., Int. Ed.*, 2016, **55**, 4087–4091.
20 N. Campagnol, R. Romero-Vara, W. Deleu, L. Stappers, K. Binnemans, D. E. De Vos and J. Fransaer, *ChemElectroChem*, 2014, **1**, 1182–1188.

21 F. Cao, M. Zhao, Y. Yu, B. Chen, Y. Huang, J. Yang, X. Cao, Q. Lu, X. Zhang, Z. Zhang, C. Tan and H. Zhang, *J. Am. Chem. Soc.*, 2016, **138**, 6924–6927.
22 J.-C. Tan, P. J. Saines, E. G. Bithell and A. K. Cheetham, *ACS Nano*, 2012, **6**, 615–621.
23 S. C. Junggeburth, L. Diehl, S. Werner, V. Duppel, W. Sigle and B. V. Lotsch, *J. Am. Chem. Soc.*, 2013, **135**, 6157–6164.
24 T. De Baerdemaeker, M. Feyen, T. Vanbergen, U. Müller, B. Yilmaz, F.-S. Xiao, W. Zhang, T. Yokoi, X. Bao, D. E. De Vos and H. Gies, *Chem. Mater.*, 2015, **27**, 316–326.
25 C. Hermosa, B. R. Horrocks, J. I. Martinez, F. Liscio, J. Gomez-Herrero and F. Zamora, *Chem. Sci.*, 2015, **6**, 2553–2558.
26 A. Gallego, C. Hermosa, O. Castillo, I. Berlanga, C. J. Gómez-García, E. Mateo-Martí, J. I. Martínez, F. Flores, C. Gómez-Navarro, J. Gómez-Herrero, S. Delgado and F. Zamora, *Adv. Mater.*, 2013, **25**, 2141–2146.
27 R. R. Salunkhe, J. Tang, Y. Kamachi, T. Nakato, J. H. Kim and Y. Yamauchi, *ACS Nano*, 2015, **9**, 6288–6296.
28 R. Li, Z. Lin, X. Ba, Y. Li, R. Ding and J. Liu, *Nanoscale Horiz.*, 2016, **1**, 150–155.
29 R. Li, Y. Wang, C. Zhou, C. Wang, X. Ba, Y. Li, X. Huang and J. Liu, *Adv. Funct. Mater.*, 2015, **25**, 5384–5394.
30 J. Liu, C. Guan, C. Zhou, Z. Fan, Q. Ke, G. Zhang, C. Liu and J. Wang, *Adv. Mater.*, 2016, **28**, 8732–8739.
31 C. Wang, L. Wu, H. Wang, W. Zuo, Y. Li and J. Liu, *Adv. Funct. Mater.*, 2015, **25**, 3524–3533.
32 Z. Liu, J. Xu, D. Chen and G. Shen, *Chem. Soc. Rev.*, 2015, **44**, 161–192.
33 X. Lu, M. Yu, G. Wang, Y. Tong and Y. Li, *Energy Environ. Sci.*, 2014, **7**, 2160–2181.
34 Y. Zhang, W. Bai, X. Cheng, J. Ren, W. Weng, P. Chen, X. Fang, Z. Zhang and H. Peng, *Angew. Chem., Int. Ed.*, 2014, **53**, 14564–14568.
35 Y. Meng, Y. Zhao, C. Hu, H. Cheng, Y. Hu, Z. Zhang, G. Shi and L. Qu, *Adv. Mater.*, 2013, **25**, 2326–2331.
36 N.-S. Choi, Z. Chen, S. A. Freunberger, X. Ji, Y.-K. Sun, K. Amine, G. Yushin, L. F. Nazar, J. Cho and P. G. Bruce, *Angew. Chem., Int. Ed.*, 2012, **51**, 9994–10024.
37 G. Wang, L. Zhang and J. Zhang, *Chem. Soc. Rev.*, 2012, **41**, 797–828.
38 M. F. El-Kady, Y. Shao and R. B. Kaner, *Nat. Rev. Mater.*, 2016, **1**, 16033.
39 P. Yang and W. Mai, *Nano Energy*, 2014, **8**, 274–290.
40 J. Ni, S. Fu, C. Wu, J. Maier, Y. Yu and L. Li, *Adv. Mater.*, 2016, **28**, 2259–2265.
41 L. Wang, X. Feng, L. Ren, Q. Piao, J. Zhong, Y. Wang, H. Li, Y. Chen and B. Wang, *J. Am. Chem. Soc.*, 2015, **137**, 4920–4923.
42 T. Y. Ma, S. Dai, M. Jaroniec and S. Z. Qiao, *J. Am. Chem. Soc.*, 2014, **136**, 13925–13931.
43 D. Ye, G. Zeng, K. Nogita, K. Ozawa, M. Hankel, D. J. Searles and L. Wang, *Adv. Funct. Mater.*, 2015, **25**, 7488–7496.
44 D. Kong, W. Ren, C. Cheng, Y. Wang, Z. Huang and H. Y. Yang, *ACS Appl. Mater. Interfaces*, 2015, **7**, 21334–21346.
45 P. Xiong, J. Zhu, L. Zhang and X. Wang, *Nanoscale Horiz.*, 2016, **1**, 340–374.
46 A. L. M. Reddy, S. R. Gowda, M. M. Shaijumon and P. M. Ajayan, *Adv. Mater.*, 2012, **24**, 5045–5064.
47 R. Chen, J. Yao, Q. Gu, S. Smeets, C. Baerlocher, H. Gu, D. Zhu, W. Morris, O. M. Yaghi and H. Wang, *Chem. Commun.*, 2013, **49**, 9500–9502.
48 M.-H. Sun, S.-Z. Huang, L.-H. Chen, Y. Li, X.-Y. Yang, Z.-Y. Yuan and B.-L. Su, *Chem. Soc. Rev.*, 2016, **45**, 3479–3563.
49 Q. Liao, N. Li, S. Jin, G. Yang and C. Wang, *ACS Nano*, 2015, **9**, 5310–5317.
50 S. Han, D. Wu, S. Li, F. Zhang and X. Feng, *Adv. Mater.*, 2013, **26**, 849–864.
51 H. Tang, S. Cai, S. Xie, Z. Wang, Y. Tong, M. Pan and X. Lu, *Adv. Sci.*, 2016, **3**, DOI: 10.1002/advs.201500265.
52 Y. Cheng, L. Huang, X. Xiao, B. Yao, L. Yuan, T. Li, Z. Hu, B. Wang, J. Wan and J. Zhou, *Nano Energy*, 2015, **15**, 66–74.
53 Z.-S. Wu, A. Winter, L. Chen, Y. Sun, A. Turchanin, X. Feng and K. Müllen, *Adv. Mater.*, 2012, **24**, 5130–5135.
54 Y. M. Chen, L. Yu and X. W. Lou, *Angew. Chem.*, 2016, **128**, 6094–6097.
55 Y. Fan, N. Zhang, L. Zhang, H. Shao, J. Wang, J. Zhang and C. Cao, *J. Electrochem. Soc.*, 2013, **160**, F218–F223.
56 X. Wang, F. Wang, L. Wang, M. Li, Y. Wang, B. Chen, Y. Zhu, L. Fu, L. Zha, L. Zhang, Y. Wu and W. Huang, *Adv. Mater.*, 2016, **28**, 4904–4911.
57 Y. Wang, T. Zhou, K. Jiang, P. Da, Z. Peng, J. Tang, B. Kong, W.-B. Cai, Z. Yang and G. Zheng, *Adv. Energy Mater.*, 2014, **4**, 1400696.
58 G. Huang, F. Zhang, X. Du, Y. Qin, D. Yin and L. Wang, *ACS Nano*, 2015, **9**, 1592–1599.
59 J. Wei, Y. Hu, Y. Liang, B. Kong, J. Zhang, J. Song, Q. Bao, G. P. Simon, S. P. Jiang and H. Wang, *Adv. Funct. Mater.*, 2015, **25**, 5768–5777.
60 M. Jiang, X. Cao, D. Zhu, Y. Duan and J. Zhang, *Electrochim. Acta*, 2016, **196**, 699–707.
61 D. Kong, C. Cheng, Y. Wang, J. I. Wong, Y. Yang and H. Y. Yang, *J. Mater. Chem. A*, 2015, **3**, 16150–16161.
62 C. Feng, J. Zhang, Y. He, C. Zhong, W. Hu, L. Liu and Y. Deng, *ACS Nano*, 2015, **9**, 1730–1739.
63 C. Guan, X. Qian, X. Wang, Y. Cao, Q. Zhang, A. Li and J. Wang, *Nanotechnology*, 2015, **26**, 094001.
64 H. Wang, Y. Zhang, H. Ang, Y. Zhang, H. T. Tan, Y. Zhang, Y. Guo, J. B. Franklin, X. L. Wu, M. Srinivasan, H. J. Fan and Q. Yan, *Adv. Funct. Mater.*, 2016, **26**, 3082–3093.
65 J. Xu, Z. Tan, W. Zeng, G. Chen, S. Wu, Y. Zhao, K. Ni, Z. Tao, M. Ikram, H. Ji and Y. Zhu, *Adv. Mater.*, 2016, **28**, 5222–5228.
66 J. Tang, P. Yuan, C. Cai, Y. Fu and X. Ma, *Adv. Energy Mater.*, 2016, **6**, 1600813.
67 C. Long, D. Qi, T. Wei, J. Yan, L. Jiang and Z. Fan, *Adv. Funct. Mater.*, 2014, **24**, 3953–3961.
68 X. Xu, M. Wang, Y. Liu, Y. Li, T. Lu and L. Pan, *Energy Storage Mater.*, 2016, **5**, 132–138.

69 R. R. Salunkhe, C. Young, J. Tang, T. Takei, Y. Ide, N. Kobayashi and Y. Yamauchi, *Chem. Commun.*, 2016, **52**, 4764–4767.
70 X. Cao, B. Zheng, W. Shi, J. Yang, Z. Fan, Z. Luo, X. Rui, B. Chen, Q. Yan and H. Zhang, *Adv. Mater.*, 2015, **27**, 4695–4701.
71 P. Wen, Z. Li, P. Gong, J. Sun, J. Wang and S. Yang, *RSC Adv.*, 2016, **6**, 13264–13271.
72 H. Hu, B. Guan, B. Xia and X. W. Lou, *J. Am. Chem. Soc.*, 2015, **137**, 5590–5595.
73 Z. Bi, M. P. Paranthaman, P. A. Menchhofer, R. R. Dehoff, C. A. Bridges, M. Chi, B. Guo, X.-G. Sun and S. Dai, *J. Power Sources*, 2013, **222**, 461–466.
74 J. Yang, F. Wei, Y. Sui, J. Qi, Y. He, Q. Meng and S. Zhang, *RSC Adv.*, 2016, **6**, 61803–61808.